Neuron
Article

p73 Regulates Neurodegeneration and Phospho-Tau Accumulation during Aging and Alzheimer's Disease

Monica K. Wetzel,[1,2] Sibel Naska,[1,2] Christine L. Laliberté,[1] Vladimir V. Rymar,[5] Masashi Fujitani,[1,2] Jeffrey A. Biernaskie,[2] Christy J. Cole,[3,6] Jason P. Lerch,[4] Shoshana Spring,[4] S.-H. Wang,[3] Paul W. Frankland,[3,6] R. Mark Henkelman,[4,7] Sheena A. Josselyn,[3,6] Abbas F. Sadikot,[5] Freda D. Miller,[2,6,8,*] and David R. Kaplan[1,8]
[1]Cell Biology
[2]Developmental and Stem Cell Biology
[3]Neuroscience and Mental Health
[4]Mouse Imaging Groups, Hospital for Sick Children
[5]Division of Neurosurgery
Montreal Neurological Institute, McGill University, Montreal, Quebec, Canada H3A 2B4
[6]Department of Physiology
[7]Department of Medical Biophysics
[8]Department of Molecular Genetics
University of Toronto, Toronto, Canada M5G 1X5
*Correspondence: fredam@sickkids.ca
DOI 10.1016/j.neuron.2008.07.021

SUMMARY

The genetic mechanisms that regulate neurodegeneration are only poorly understood. We show that the loss of one allele of the p53 family member, p73, makes mice susceptible to neurodegeneration as a consequence of aging or Alzheimer's disease (AD). Behavioral analyses demonstrated that old, but not young, $p73^{+/-}$ mice displayed reduced motor and cognitive function, CNS atrophy, and neuronal degeneration. Unexpectedly, brains of aged $p73^{+/-}$ mice demonstrated dramatic accumulations of phospho-tau (P-tau)-positive filaments. Moreover, when crossed to a mouse model of AD expressing a mutant amyloid precursor protein, brains of these mice showed neuronal degeneration and early and robust formation of tangle-like structures containing P-tau. The increase in P-tau was likely mediated by JNK; in $p73^{+/-}$ neurons, the activity of the p73 target JNK was enhanced, and JNK regulated P-tau levels. Thus, p73 is essential for preventing neurodegeneration, and haploinsufficiency for *p73* may be a susceptibility factor for AD and other neurodegenerative disorders.

INTRODUCTION

The cellular mechanisms that regulate nervous system degeneration during aging or in neurodegenerative disorders are only poorly understood, in spite of their clinical importance. For example, much of what we know regarding neural cell death comes from studies of naturally occurring developmental death or injury-induced death, but the relevance of these relatively well-understood apoptotic mechanisms to aging or neurodegeneration is still an open question (for example, see Dusart et al., 2006; Zhu et al., 2006). Moreover, the pathology observed in many neurodegenerative disorders indicates that neurons accumulate intracellular protein aggregates and/or cellular damage that leads to their slow degeneration and death, as opposed to a rapid and controlled apoptotic suicide. Instead, increasing evidence indicates that, in the aged or degenerating nervous system, prolonged exposure to relatively minor insults leads to cumulative neuronal oxidative stress and/or DNA damage, which in turn causes neurons to senesce, reenter the cell cycle and/or atrophy, and ultimately degenerate (Lin and Beal, 2006; Herrup and Yang, 2007). Thus, both the cause and the enactment of neuronal cell death differ during development versus aging or degeneration.

While many neurodegenerative disorders appear to be much more than just accelerated aging, several lines of evidence suggest some similarities. For example, overexpression in *Drosophila* motor neurons of SOD1, one gene that is mutated in familial amyotrophic lateral sclerosis (ALS), significantly extends fly lifespan (Parkes et al., 1998). Moreover, brains of some aged, apparently normal individuals display neurodegenerative hallmarks such as P-PHF-tau neurofibrillary tangles (Imhof et al., 2007). Thus, perturbations that accelerate neural aging may contribute to and/or predispose individuals to neurodegenerative disorders.

In this regard, the tumor suppressor p53 and its family member, p63, have been implicated in aging outside of the nervous system; mouse models with enhanced p53 activity display accelerated aging and decreased lifespan (Tyner et al., 2002; Lavigueur et al., 1989; Maier et al., 2004), and aging is enhanced in $p63^{+/-}$ mice (Keyes et al., 2005). These phenotypes are thought to occur as a consequence of disruptions in p53 family-mediated regulation of genomic stability and cellular senescence, which in turn impact on cellular/organismic aging (reviewed in Papazoglu and Mills, 2007). While aging phenotypes in these mice were nonneural, they raise the possibility that the third p53 family member, p73, which is enriched in the PNS and CNS (Yang et al., 2000; Pozniak et al., 2000), might play an analogous role in the nervous system. However, although

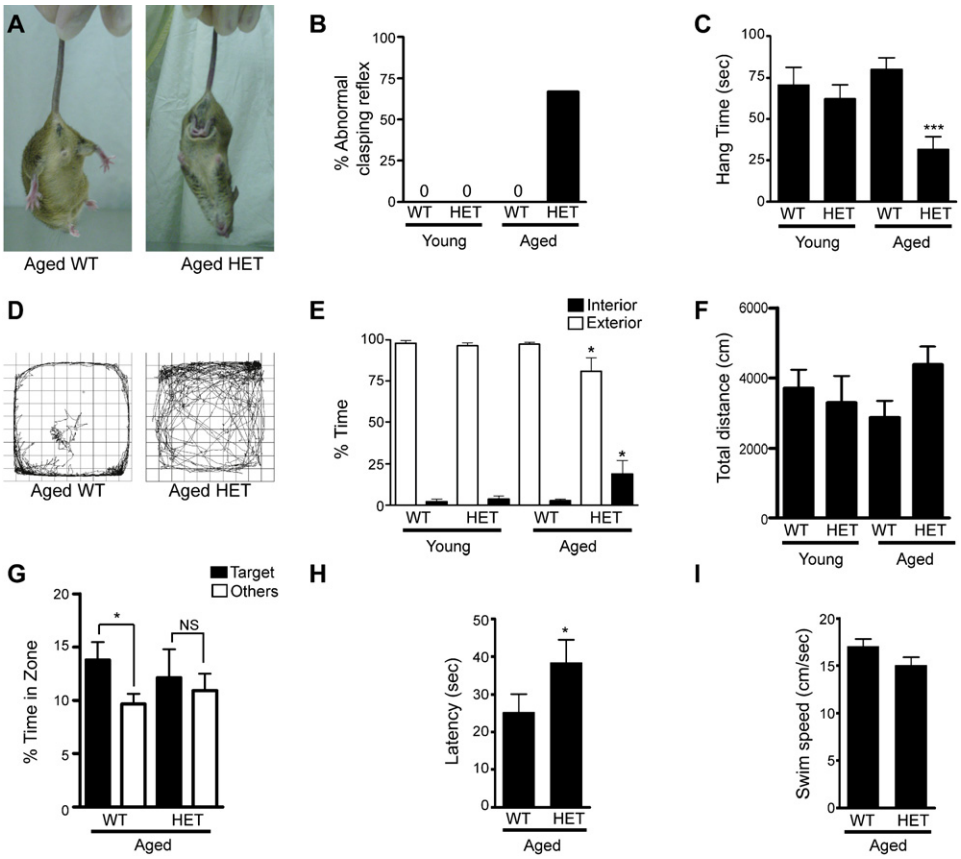

Figure 1. Aged $p73^{+/-}$ Mice Display Behavioral Changes Indicative of Neurodegeneration

(A) Photographs showing the normal clasping behavior of an aged, wild-type, $p73^{+/+}$ mouse and the abnormal clasping behavior of an aged, $p73^{+/-}$ mouse. Note that the $p73^{+/-}$ mouse draws its limbs into its body rather than splaying them away from its trunk.

(B) Quantification of the percentage of young or aged $p73^{+/+}$ versus $p73^{+/-}$ mice displaying the abnormal clasping behavior shown in (A).

(C–F) Young (3-month-old) and aged (17-month-old) male $p73^{+/+}$ and $p73^{+/-}$ mice were tested for behavioral changes associated with neurodegeneration (n = 13 young $p73^{+/+}$, 15 young $p73^{+/-}$, 16 aged $p73^{+/+}$, and 12 aged $p73^{+/-}$ mice). (C) The mean time mice spent hanging from a suspended grid. Mice were tested three times, and the maximum time was recorded. (D–F) Results of the open-field test, showing representative traces of open-field exploration during a 30 min trial (D), the mean percent time spent in the interior versus exterior of the open field (E), and the mean total distance traveled during the trial (F).

(G–I) Results of the Morris water maze test, showing the mean percent time spent in the target versus nontarget zone during the probe test (G), the mean time to reach the platform (latency) (H), and the mean swim speed (J). (n = 16 aged $p73^{+/+}$ and n = 12 aged $p73^{+/-}$ mice).

All values are mean ± SEM. *p < 0.05, ***p < 0.001, NS = p > 0.05. In all panels, WT = $p73^{+/+}$ and HET = $p73^{+/-}$.

we previously showed that p73 is predominantly expressed as a truncated, dominant-inhibitory isoform, ΔNp73, that prevents neuronal apoptosis during development and following injury (Pozniak et al., 2000, 2002; Walsh et al., 2004), there is no evidence to suggest that p73 is important for cellular necrosis or degeneration. Nonetheless, two recent reports indicate that decreased p73 expression occurs in some cases of AD (Li et al., 2004) and that some individuals have lost one copy of the genomic locus encompassing the p73 gene (Wong et al., 2007).

Here, we have asked whether p73 might play a previously unsuspected role in neurodegeneration and show that haploinsufficiency for p73 causes age-related neurodegeneration. Moreover, we demonstrate that decreased p73 causes formation of P-PHF-tau tangle-like structures in the aged nervous system, and coincident with the formation of amyloid plaques in an amyloid-based mouse model for AD. Thus, p73 is essential to prevent neurodegeneration during aging, and heterozygosity for p73 may be a susceptibility factor for AD or other neurodegenerative disorders.

RESULTS

Normal Levels of p73 Are Essential to Prevent Behavioral Changes Indicative of Age-Related Neurodegeneration

To ask whether changes in p73 copy number would sensitize mice to neurodegeneration, we compared the behavior of young (3- to 4-month-old) and aged (16- to 18-month-old) $p73^{+/-}$ versus $p73^{+/+}$ mice. Initially, we examined an abnormal clasping behavior seen in several mouse neurodegeneration models (Liou et al., 2003; Lewis et al., 2000), where mice clasp their limbs into their bodies when picked up by their tails. Aged $p73^{+/-}$ but not $p73^{+/+}$ adults displayed this abnormal clasping behavior (Figure 1A and Movie S1 available online). Young adult $p73^{+/-}$

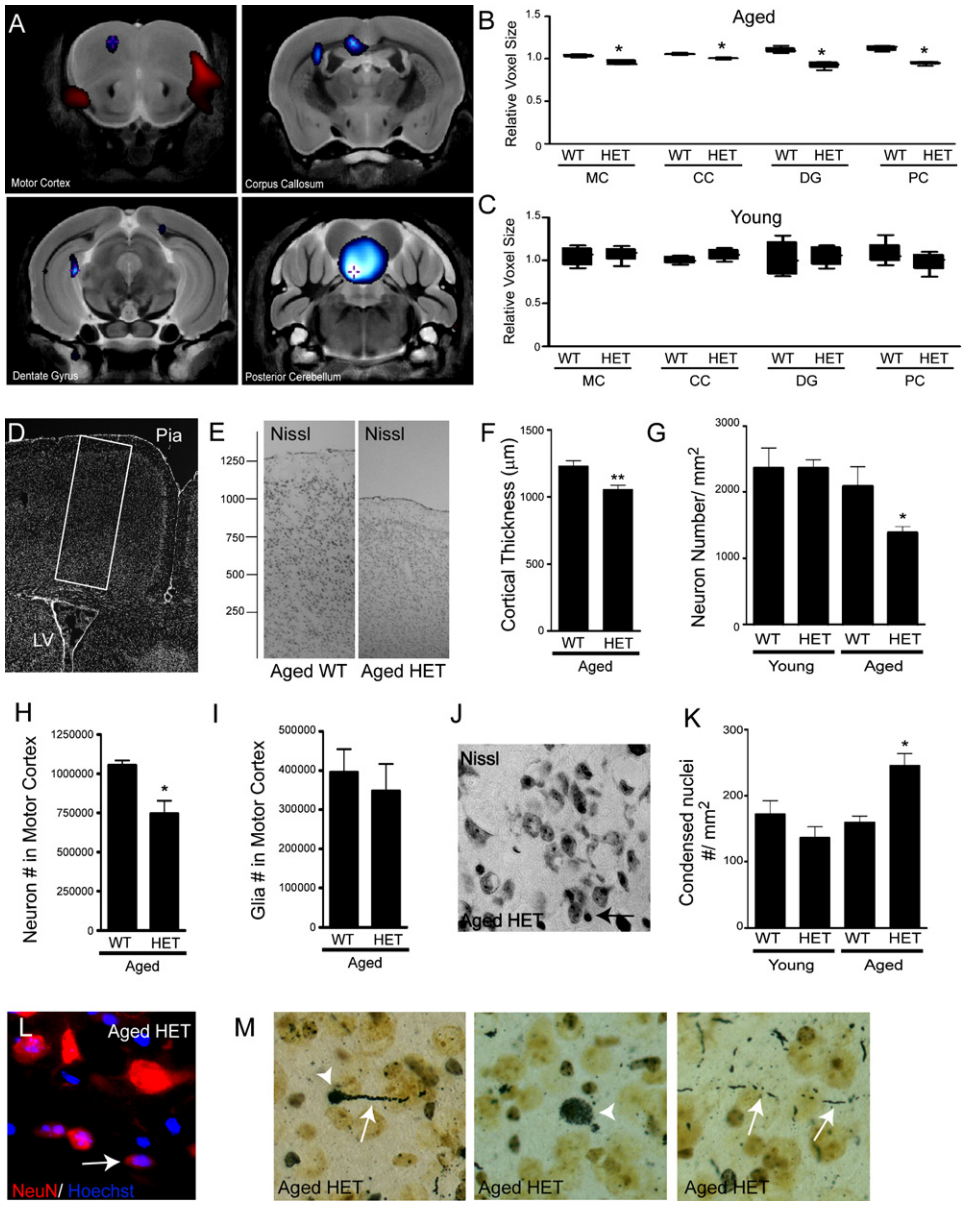

Figure 2. p73 Haploinsufficiency Causes Age-Related Neuronal Degeneration and CNS Atrophy

(A) Combined representative MR images of 5 $p73^{+/-}$ aged mouse brains where blue indicates regions that are significantly smaller and red regions that are significantly larger with over 95% certainty in aged $p73^{+/-}$ versus $p73^{+/+}$ mouse brains. The reconstruction of the entire combined brain is shown in Movie S1. The red regions encompass the space between the skull and brain, which is larger in aged $p73^{+/-}$ mice due to brain atrophy.

(B and C) The mean relative voxel size in aged (B) and young (C) brain regions identified as significantly different between $p73^{+/+}$ versus $p73^{+/-}$ mice in the MR image atlas created in (A). (n = 5 per group). All values are mean ± SEM. *p < 0.05. MC, motor cortex; CC, corpus callosum; DG, dentate gyrus; PC, posterior cerebellum.

(D) Photomicrograph of the 325 μm strip of motor cortex (boxed) that was assessed for quantification. LV, lateral ventricle.

(E) Representative photomicrographs of Nissl-stained coronal sections at the level of the motor cortex shown in (D) from aged (17-month-old) $p73^{+/+}$ and $p73^{+/-}$ brains.

(F) Mean cortical thickness as determined by measuring the distance from the corpus callosum to the pia in photomicrographs similar to those shown in (E) (n = 5 mice of each genotype).

(G) Mean density of Nissl-stained neurons in the motor cortex of aged $p73^{+/+}$ versus $p73^{+/-}$ brains (n = 5 per group).

(H) Absolute number of primary motor cortex neurons in $p73^{+/+}$ and $p73^{+/-}$ brains as determined using the optical fractionator method (*p < 0.05, n = 3 per group).

(I) Absolute number of glial cells in the primary motor cortex of $p73^{+/+}$ and $p73^{+/-}$ brains as determined using the optical fractionator method (n = 3 per group).

(J) Representative photomicrograph of a Nissl-stained section through the $p73^{+/+}$ motor cortex showing condensed cells (arrow).

(K) Mean density of small, condensed cells in the motor cortex of young and aged $p73^{+/+}$ and $p73^{+/-}$ brains (*p < 0.05, n = 5 per group).

mice were normal but acquired this behavior with time, so that almost 75% were positive by 16–18 months of age (Figure 1B).

We then performed a battery of neurological and sensory-motor assays on young and aged $p73^{+/-}$ versus $p73^{+/+}$ mice, including the sticky dot test, the elevated body swing test, the righting reflex text, the negative geotaxis test, the paw grip endurance test, a cylinder rearing test, a grid walking test, the open-field test, and gait analysis. Aged, but not young, $p73^{+/-}$ mice performed poorly on two, the paw grip endurance and open-field tests. In the former, aged $p73^{+/-}$ mice maintained their grip for a significantly shorter time than any other group, including aged $p73^{+/+}$ mice (Figure 1C). In the open-field test, aged $p73^{+/-}$ mice spent significantly more time in the center of the open field than any other group (Figures 1D and 1E), although the distance they traveled was similar (Figure 1F), suggesting a reduction in overall anxiety levels.

Since spatial learning and memory are also perturbed in mouse models of neurodegeneration, we asked whether aged $p73^{+/-}$ mice were impaired in this regard using the hidden platform version of the Morris water maze (Kobayashi and Chen, 2005). In this test, an invisible escape platform is submerged just below water level, and white curtains are marked with distinct cues, thereby allowing mice to triangulate the hidden platform location. Mice were trained to find the platform and assessed on their ability to spatially learn and remember the platform location. Aged $p73^{+/-}$ mice were significantly impaired in their ability to discriminate the platform location (as measured by percent time in the platform zone) and in the length of time (latency) it took to find the platform (Figures 1G and 1H), although they swam at a speed similar to aged $p73^{+/+}$ mice (Figure 1I). In contrast, young $p73^{+/-}$ and $p73^{+/+}$ mice behaved similarly on this test (data not shown). Thus, aged $p73^{+/-}$ mice displayed a number of behaviors diagnostic of age-related neurodegeneration.

$p73^{+/-}$ Mice Show Anatomical Evidence of Age-Related Neurodegeneration

To ask about neuroanatomical perturbations that might cause these behavioral abnormalities, we performed 3D magnetic resonance imaging (MRI) and computer analysis. Digital images from within the skulls of perfused young and aged $p73^{+/+}$ and $p73^{+/-}$ murine mice were acquired with a multichannel 7.0 Tesla MRI scanner, allowing for resolution and volume analysis of fine nuclei and white matter tracts. Computer analysis created an unbiased model-independent atlas of all MR scans, which were deformed into exact alignment with each other in an unbiased fashion; quantitative volume differences of individual mouse neuroanatomical features were determined based upon this collective brain atlas. This analysis revealed that, relative to aged $p73^{+/+}$ mice, aged $p73^{+/-}$ mice displayed a 5%–16% reduction in volume of selected brain regions, including the motor cortex, corpus callosum, hippocampal dentate gyrus, and posterior cerebellum (Figures 2A and 2B and Movie S2). In contrast, young $p73^{+/-}$ versus $p73^{+/+}$ brains were statistically similar in all these regions (Figure 2C). The volume perturbations in motor cortex and cerebellum could explain the aberrant clasping and grip test behaviors, and the dentate gyrus atrophy could explain the poor water maze performance.

To ask about the cellular basis of this atrophy, we analyzed cytoarchitecture of Nissl-stained sections through one affected region, the motor cortex. Measurement of coronal sections at equivalent rostrocaudal levels revealed that width of the motor cortex from corpus callosum to the pia (see boxed region in Figure 2D) was thinner in aged $p73^{+/-}$ versus $p73^{+/+}$ mice (Figures 2E and 2F). Neuronal density was also decreased in aged $p73^{+/-}$ mice (Figure 2G). To confirm this, we performed unbiased stereology using the optical fractionator method (Gundersen et al., 1988; West et al., 1996; Luk and Sadikot, 2003; Luk et al., 2001). The mean coefficient of error (Gundersen and Jensen, 1987) of Nissl-stained neuronal counts was 0.9 ± 0.005 (n = 4). In aged $p73^{+/-}$ primary motor cortex, there was a reduction (29%) in total neuron number (743,531 ± 83,667 versus 1,054,281 ± 30,512 in aged controls, mean ± SEM, n = 3; $p < 0.05$) (Figure 2H) and in total volumetric density (28%; 129,144 ± 7,967 versus 179,535 ± 12,601 in aged controls; number/mm^3, mean ± SEM, n = 3; $p < 0.05$). In contrast, total glial cell number was unchanged (Figure 2I).

We also observed an increase in density of small, condensed cells in the aged $p73^{+/-}$ motor cortex (Figures 2J and 2K). Some of these expressed the neuronal marker NeuN (Figure 2L), but not the astrocytic marker GFAP or the microglial marker Iba1 (data not shown). To ask whether these were dying neurons, we performed silver staining for degenerating cells. This analysis revealed, in aged $p73^{+/-}$ but not $p73^{+/+}$ brains, condensed, silver-stained, degenerating cells, many with dystrophic neurites (Figure 2M), identifying them as neurons. There were also many silver-stained neuritic processes (Figure 2M). In contrast, young $p73^{+/-}$ and $p73^{+/+}$ brains did not contain degenerating cells (data not shown), and both genotypes were similar with regard to cortical thickness ($p > 0.05$) and density of neurons and condensed cells (Figures 2G and 2K). Thus, neuronal degeneration likely accounts for the atrophy of aged $p73^{+/-}$ brains.

Neurodegenerative disorders like Parkinson's disease and AD also manifest in the PNS (Hawkes, 2006; Goldstein, 2003). In this regard, we observed that 67% of aged $p73^{+/-}$, but not $p73^{+/+}$, mice displayed prolapse of the penis and/or rectum (12/21 penis only, 4/21 rectum only, 2/21 both; Figure S1A). To ask whether this was due to peripheral neurodegeneration, we characterized parasympathetic neurons of the major pelvic ganglion, which innervates the penis. Immunostaining for the parasympathetic marker nNOS and the panneuronal marker PGP9.5 revealed that pelvic ganglia from aged prolapsed $p73^{+/-}$ mice contained many fewer neurons (Figures S1B and S1C), and those neurons that were present were shrunken. Thus, $p73^{+/-}$ mice displayed phenotypes arising from degeneration of both the CNS and PNS.

(L) Immunostaining for NeuN (red) in the motor cortex showing that some of the condensed cells are shrunken, potentially degenerating, neurons (arrow). Section was counterstained with Hoechst to show nuclei (blue).

(M) Photomicrographs of silver-stained $p73^{+/-}$ cortices, showing argyrophilic, degenerating condensed neurons with processes (left panel), larger degenerating cells (middle panel), and degenerating neuritic processes (right panel).

In all panels, arrowheads denote cell bodies, and arrows degenerating neuritic processes. In all panels, WT = $p73^{+/+}$, and HET = $p73^{+/-}$.

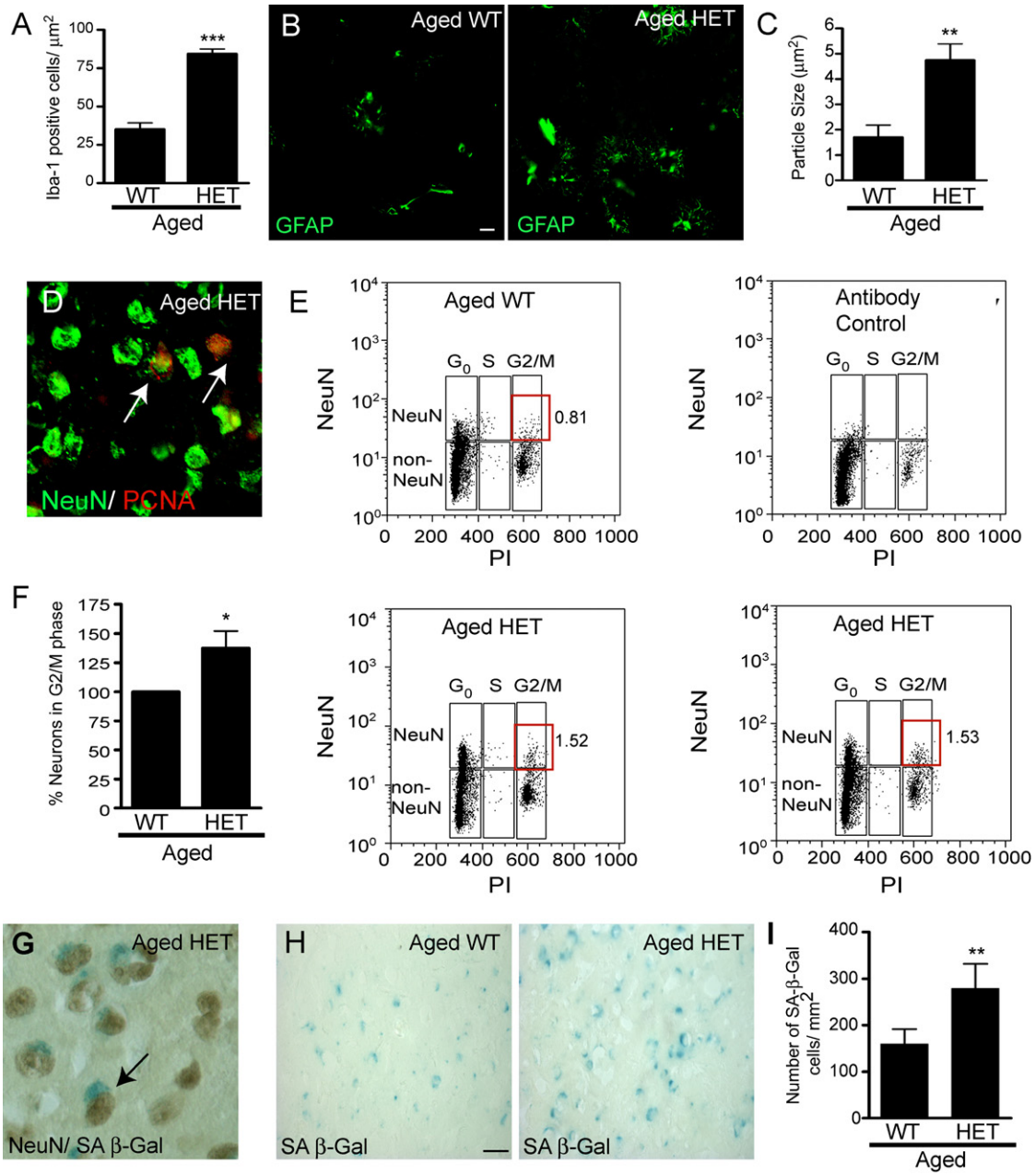

Figure 3. Aged $p73^{+/-}$ Brains Display Hallmarks of Neurodegeneration

(A) Mean density of microglia in the motor cortex of aged $p73^{+/+}$ versus $p73^{+/-}$ mice (n = 5 per group).

(B) Representative photomicrographs of sections through the aged $p73^{+/+}$ (Aged WT) and $p73^{+/-}$ (Aged HET) motor cortex immunostained for the reactive astrocyte marker GFAP (green).

(C) Relative mean lipofuscin particle size in the motor cortex of aged $p73^{+/+}$ versus $p73^{+/-}$ mice (n = 5 per group).

(D) Photomicrograph of neurons within the motor cortex immunostained for NeuN (green) and PCNA (red). Arrows indicate double-labeled cells.

(E) Representative flow cytometry plots of cortical cells from aged $p73^{+/+}$ versus $p73^{+/-}$ brains stained with neuron-specific NeuN (y axis) and with propidium iodide (PI, x axis) to assess neuronal DNA content. The antibody control, where primary antibody was omitted, but propidium iodide was included, is shown for comparison. The red boxes indicate the relevant NeuN-positive population, and numbers to the right of these boxes indicate the percentage of total cells that were NeuN positive and that had a DNA content indicative of G2 or M phase.

(F) Flow cytometry plots similar to those shown in (E) were used to determine the normalized relative percentage of neurons in the G2/M phase of the cell cycle (n = 6 per group). The proportion of neurons in the aged $p73^{+/+}$ cortex that were in G2/M phase was considered to be 100%.

(G) Photomicrograph of neurons in the motor cortex stained for SA-β-galactosidase (blue) and then immunostained for NeuN (brown).

(H) Representative photomicrographs of staining for the senescence marker SA-β-galactosidase (blue) in aged $p73^{+/+}$ and $p73^{+/-}$ motor cortex, showing the more lightly staining cells that were quantified.

Aged $p73^{+/-}$ Brains Display Microglial Activation and Lipofuscin Accumulation

Since neurodegenerative disorders such as AD display activation of microglia and astrocytes, we asked whether similar changes might occur in aged $p73^{+/-}$ brains. Immunostaining for Iba-1 revealed increased microglial density throughout aged $p73^{+/-}$ versus $p73^{+/+}$ brains, and quantification within a 325 μm wide strip of motor cortex spanning from the corpus callosum to the pia (see Figure 2D) demonstrated an increase of ~3-fold (Figures 3A and S2A). Similarly, immunostaining for GFAP showed increased reactive astrocytes in the aged $p73^{+/-}$ motor cortex (Figure 3B).

Another hallmark of neurodegeneration is intralysosomal accumulation of the oxidative stress biomarker lipofuscin, a cause of premature dementia in Batten's disease (Seehafer and Pearce, 2006; Haltia et al., 2006). Lipofuscin autofluorescence was increased throughout aged $p73^{+/-}$ versus $p73^{+/+}$ brains (Figure S2B), and quantification demonstrated an ~2.5-fold increase in lipofuscin particle size in the aged $p73^{+/-}$ motor cortex (Figure 3C). Thus, normal levels of p73 are necessary to prevent brains from degenerating as they age.

Normal Levels of p73 Are Essential to Prevent Neuronal Cell Cycle Reentry and Cellular Senescence during Aging

One pathological event observed in AD is aberrant re-expression of cell cycle proteins and re-entry of neurons into the cell cycle (Herrup and Yang, 2007). Since p73 can directly regulate the cell cycle (Talos et al., 2007), we asked whether this also occurred in aged $p73^{+/-}$ mice. Immunostaining of forebrain sections revealed a subpopulation of NeuN-positive neurons that aberrantly expressed the cell cycle marker PCNA in the motor cortex and adjacent lateral cortical region of aged $p73^{+/-}$ but not $p73^{+/+}$ mice (Figure 3D). To confirm and quantify this result, we isolated cerebral cortices, immunostained the triturated cortical tissue for NeuN, stained with propidium iodide to monitor cell cycle status, and performed flow cytometry, gating for single cells. Approximately 0.8% of wild-type neurons had a DNA content indicative of the G_2 or M phase of the cell cycle (Figure 3E), a number that was increased as much as 2-fold with $p73^{+/-}$ neurons (Figures 3E and 3F). In contrast, the percentage of NeuN-negative nonneuronal cells in G2/M phase was similar in both genotypes ($p > 0.05$). Thus, p73 regulates neuronal cell cycle reentry as mice age.

Cellular senescence also occurs as cells and animals age, and the p53 family, including p73, is implicated in regulation of senescence (Keyes et al., 2005; Talos et al., 2007; Papazoglu and Mills, 2007). We therefore double labeled forebrain sections for NeuN and for a marker of senescing cells, senescence-associated β-galactosidase (SA-β-Gal) (Serrano et al., 1997). Two populations of SA-β-Gal-positive cells were seen in the aged cortex; NeuN-positive neurons (Figure 3G) and NeuN-negative, vasculature-associated cells that were more darkly stained for SA-β-Gal. Quantification revealed a significant increase in the more lightly stained cells in aged $p73^{+/-}$ versus $p73^{+/+}$ motor cortex (Figures 3H and 3I). Thus, p73 haploinsufficiency causes increased neuronal expression of a senescence marker as animals age.

Haploinsufficiency for p73 Causes Formation of Aberrant Phosphorylated Tau Filaments in the Aged Brain

In humans, high levels of filamentous hyperphosphorylated tau protein are thought to be one of the underlying causes of neurodegeneration (Ballatore et al., 2007). We therefore immunostained sections from brains of young and aged $p73^{+/-}$ and $p73^{+/+}$ mice with three antibodies that recognize phospho-tau-containing paired helical filaments (P-PHF-tau), AT-8 (phospho-Ser202 and phospho-Thr205; Goedert et al., 1995), AT-180 (phospho-Thr231), and AT-100 (phospho-Ser212 and phospho-Thr214). No P-PHF-tau immunoreactivity was observed in brains of young animals or of aged $p73^{+/+}$ mice (Figure 4A). Unexpectedly, all of the aged $p73^{+/-}$ brains contained abundant P-PHF-tau immunoreactivity, as visualized with the three antibodies (Figures 4A–4D). Phosphatase treatment abolished this immunostaining (Figure S3A), confirming the labeling specificity. This P-PHF-tau immunoreactivity was localized throughout the brain, including the motor cortex (Figures 4A–4D), the hippocampus, the subiculum, (Figure 4E), and the piriform cortex (data not shown). P-PHF-tau immunoreactivity was localized within cells and their neuritic processes (Figures 4A–4E), and many positive cells coexpressed βIII-tubulin (data not shown), confirming their identity as neurons. P-PHF-tau immunoreactivity was also present within neuropil threads and dystrophic neurites. Quantification within a defined region of the lateral cortex where P-PHF-tau structures were consistently present (Figure 4F) demonstrated the specificity of this immunoreactivity for aged, $p73^{+/-}$ brains (Figures 4G and 4H). In contrast, β-amyloid-positive plaques, as detected by thioflavin-T staining, were not present in brains of either genotype (data not shown).

Two different approaches confirmed that this staining reflected P-PHF-tau filaments. First, immuno-electron microscopy with AT-8 on aged $p73^{+/-}$ cortices revealed immunoreactive filaments, either scattered or in bundles, within neuronal cell bodies (Figure 4I) and axons (Figure 4J). Second, we fractionated $p73^{+/-}$ versus $p73^{+/+}$ brains to enrich for P-PHF-tau filaments (Ikeda et al., 2005); western blots confirmed the presence of AT-8-immunopositive P-PHF-tau filaments in these fractions (Figure S3B). Thus, p73 haploinsufficiency causes formation of P-PHF-tau tangle-like structures similar to those seen in neurodegenerative disorders.

Haploinsufficiency for p73 Causes Neurodegeneration and Early Formation of Phospho-Tau-Containing Filaments in an Amyloid-Based Alzheimer's Disease Model

The hallmarks of human AD are β-amyloid-positive plaques, P-PHF-tau-positive tangles, and neurodegeneration. However, most amyloid precursor protein (APP)-based mouse models show plaques, but not neurodegeneration, and if they do

(I) Mean density of SA-β-galactosidase-positive cells in the motor cortex (n = 5 per group).
All values are mean ± SEM. *$p < 0.05$, **$p < 0.01$, ***$p < 0.001$. In all panels, WT = $p73^{+/+}$, and HET = $p73^{+/-}$. Scale bar, 10 μm.

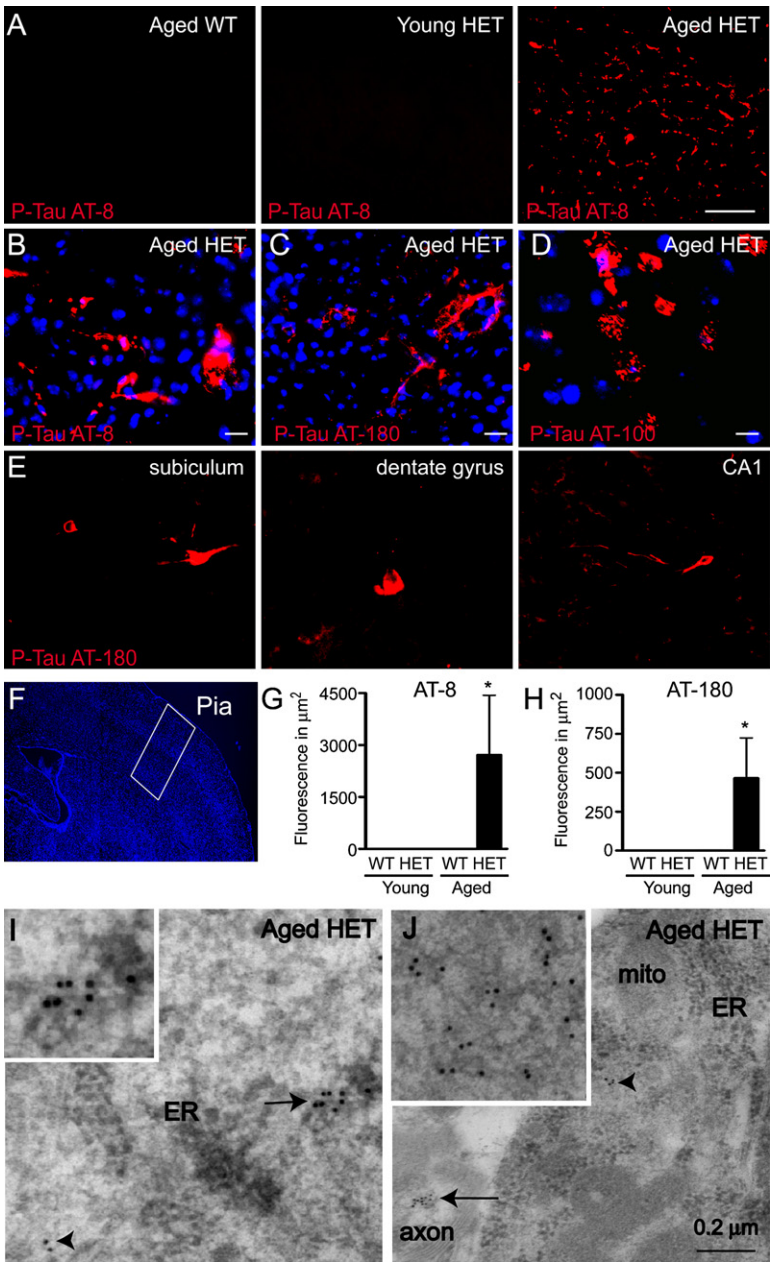

Figure 4. p73 Haploinsufficiency Leads to Accumulation of P-PHF-Tau Filaments in the Aged Brain

(A) Representative photomicrographs of coronal sections of the aged $p73^{+/+}$, young and aged $p73^{+/-}$ lateral cortex immunostained with P-PHF-tau AT-8 antibody.

(B–D) Aged $p73^{+/-}$ brain sections labeled with three different antibodies for P-PHF-tau (red) and Hoechst nuclear dye (blue), AT-8 (B), AT-180 (C), and AT-100 (D). Scale bar, 60 µm (A), 10 µm (B and C), 2.5 µm (D).

(E) Photomicrographs of hippocampal neurons displaying somatodendritic localization of P-PHF-tau (AT-180, red) within the subiculum (left panel) dentate gyrus (center panel), and CA1 pyramidal layer (right panel).

(F–H) Quantification of P-PHF-tau immunoreactivity in the cortex (region shown in [F]) in young and aged $p73^{+/+}$ versus $p73^{+/-}$ brains, as assayed using the AT-8 (G) and AT-180 (H) antibodies (n = 4 per group). Only aged $p73^{+/-}$ brains were positive for P-PHF-tau.

(I and J) Immuno-electron microscopy was performed to detect P-PHF-tau ultrastructurally in the cerebral cortex of aged $p73^{+/-}$ mouse brains using the P-PHF-tau AT-8 antibody visualized with 10 nm gold conjugated secondary antibodies. Immunoreactivity was detected within neuronal cell bodies (I) and myelinated axons (J). In panel (I), the arrow indicates gold labeling of cell body filament aggregates, and the inset shows a higher-magnification view of these filaments. The arrowhead indicates another immunolabeled structure. In panel (J), the arrow indicates a myelinated axon, with the immunopositive filaments shown at higher magnification in the inset. The arrowhead indicates immunolabeled aggregates in a neuronal cell body. Scale bar, 0.2 µm. ER, endoplasmic reticulum; mito, mitochondrion.

All values are mean ± SEM. *p < 0.05. In all panels, WT = $p73^{+/+}$, and HET = $p73^{+/-}$.

develop tangles, this only occurs long after plaque formation. Since p73 haploinsufficiency causes both neurodegeneration and P-PHF-tau positive filaments, we asked whether it might be a susceptibility factor for AD. To do this, we crossed $p73^{+/-}$ mice with the transgenic CRND8 (TgCRND8$^{+/ø}$) mouse model of AD (Chishti et al., 2001). These mice encode a double-mutant form of APP 695 (KM670/671NL+V717F) under the control of the PrP gene promoter and develop plaques, but not tangles, by 3 months and do not display neuronal loss. We analyzed these crosses at 1.5–2 months, a time point early during plaque formation, first quantifying plaque density by thioflavin T staining and immunocytochemistry with two antibodies, the 4G8 antibody specific for human APP (Figure 5C) and the 6E10 human APP C-terminal-specific antibody (data not shown). This analysis demonstrated a small number of plaques in 1.5- to 2-month-old TgCRND8$^{+/ø}$ brains, regardless of *p73* genotype (Figures 5A–5D).

We then immunostained brains with AT-8 and AT-180 to reveal P-PHF-tau. As reported (Bellucci et al., 2007), there was no immunoreactivity detected by either antibody in young TgCRND8$^{+/ø}$ brains (Figures 5E and 5F). In contrast, all of the $p73^{+/-}$; TgCRND8$^{+/ø}$ brains displayed abundant P-PHF-tau filaments/deposits at 1.5–2 months of age (Figures 5E and 5F). These P-PHF-tau structures were consistently present in the lateral cortex and, to a lesser degree, in other forebrain regions and in the hippocampus and subiculum (Figure S4). Quantification in the lateral cortex demonstrated the specificity of these P-PHF-tau filaments for the $p73^{+/-}$; TgCRND8$^{+/ø}$ brains (Figures 5G and 5H). Thus, p73 haploinsufficiency and overexpression of mutant APP together cause P-PHF-tau accumulation early during the AD-type neuropathology.

We then asked whether p73 heterozygosity led to neuronal loss in these mice. Stereological analysis, using the optical fractionator method, demonstrated that total primary motor cortex neuron number was reduced by 22% in $p73^{+/-}$; TgCRND8$^{+/ø}$ mice versus their TgCRND8$^{+/ø}$ littermates (721,617 ± 50,757

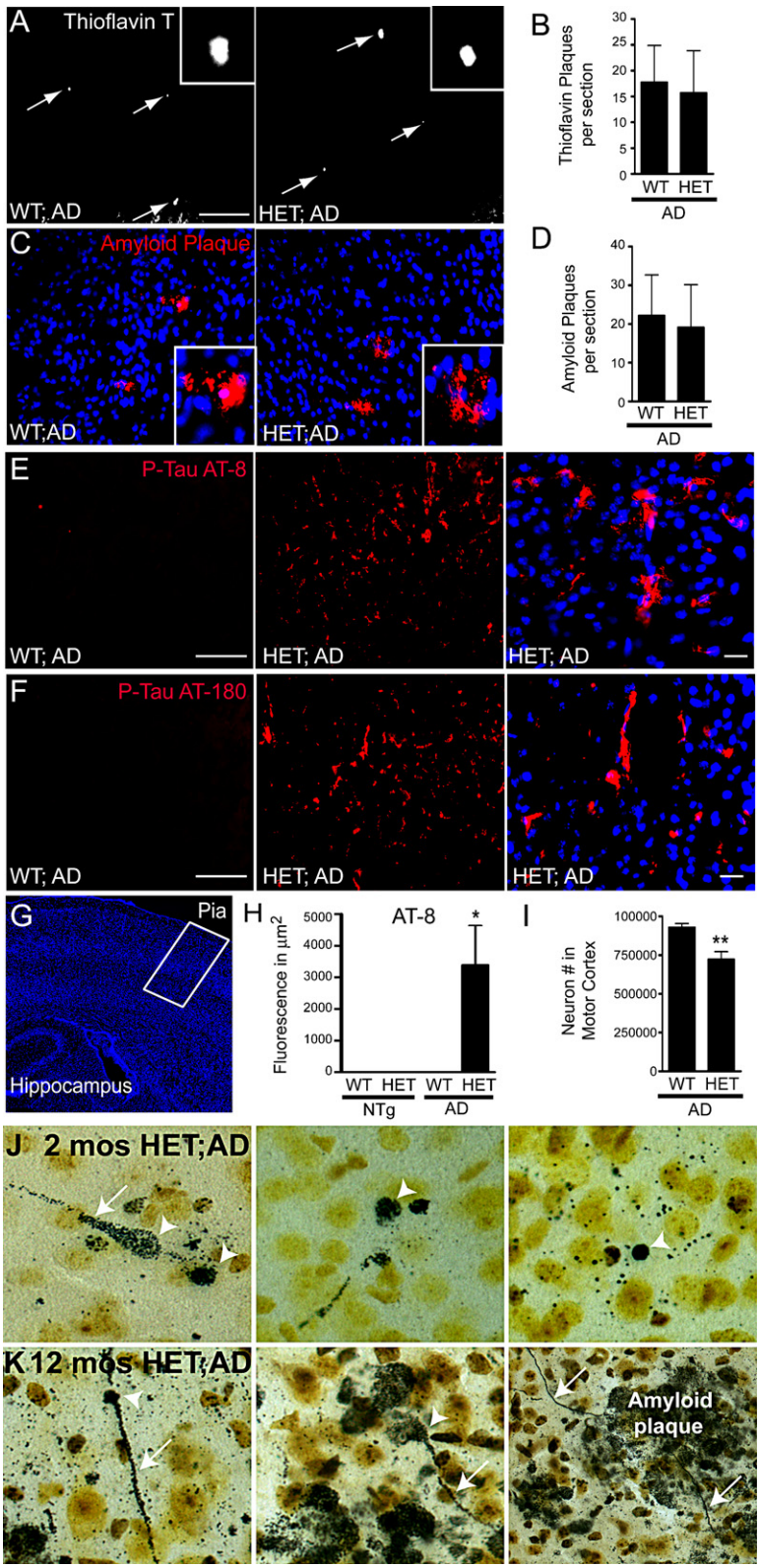

Figure 5. p73 Haploinsufficiency Causes Neuronal Degeneration and Early Formation of Phospho-Tau-Positive Filaments in TgCRND8 Mice, an AD Mouse Model

(A–D) Quantification of amyloid plaques in the cortex of 2-month-old $p73^{+/+}$;TgCRND8$^{+/\varnothing}$ (WT;AD) versus $p73^{+/-}$;TgCRND8$^{+/\varnothing}$ (HET;AD) mice, as detected and quantified using (A and B) Thioflavin T or (C and D) immunocytochemistry for human APP-specific antibody 4G8 (red), where the insets show higher-magnification micrographs of amyloid plaques. In (C), sections were counterstained with Hoechst to show nuclei (blue). Scale bar, 500 µm.

(E and F) Representative photomicrographs of coronal sections of the lateral cortex of 1.5- to 2-month-old TgCRND8 mice immunostained with two antibodies for P-PHF-tau (red), AT-8 (E) and AT-180 (F). Some panels were counterstained with Hoechst (blue). Scale bar, 60 µm (left and center panels in [E] and [F]), 10 µm (right panels in [E] and [F]).

(G–I) Quantification of P-PHF-tau immunoreactivity in the cortex (region shown in [G]) in 1.5- to 2-month-old TgCRND8$^{+/\varnothing}$ brains that were wild-type or heterozygous for the p73 gene, as assayed with the AT-8 antibody. $p73^{+/+}$ and $p73^{+/-}$ brains of the same age that did not carry the APP transgene (NTg) were also characterized. Only $p73^{+/-}$;TgCRND8$^{+/\varnothing}$ brains were positive for P-PHF-tau. n = 3 each for $p73^{+/+}$, $p73^{+/-}$, $p73^{++-}$;TgCRND8$^{+/\varnothing}$, and 4 for $p73^{+/-}$;TgCRND8$^{+/\varnothing}$. (I) Total number of primary motor cortex neurons was quantified by stereological methods for $p73^{+/-}$;TgCRND8$^{+/\varnothing}$ versus $p73^{+/-}$;TgCRND8$^{+/\varnothing}$ brains. n = 5 for each group.

(J and K) Silver staining was performed to detect argyrophilic, degenerating neurons in (J) 2-month-old and (K) 12-month-old $p73^{+/-}$;TgCRND8$^{+/\varnothing}$ brains. In all panels, arrowheads denote silver stain-positive cell bodies, while the arrows denote silver stain-positive neuritic processes. In older brains, the amyloid plaques were also silver stain-positive ([K], right panel).

All values are mean ± SEM. *p < 0.05, **p < 0.01. In all panels, WT = $p73^{+/+}$, and HET = $p73^{+/-}$; AD = TgCRND8$^{+/\varnothing}$; NTg = animals that did not carry the TgCRND8 transgene.

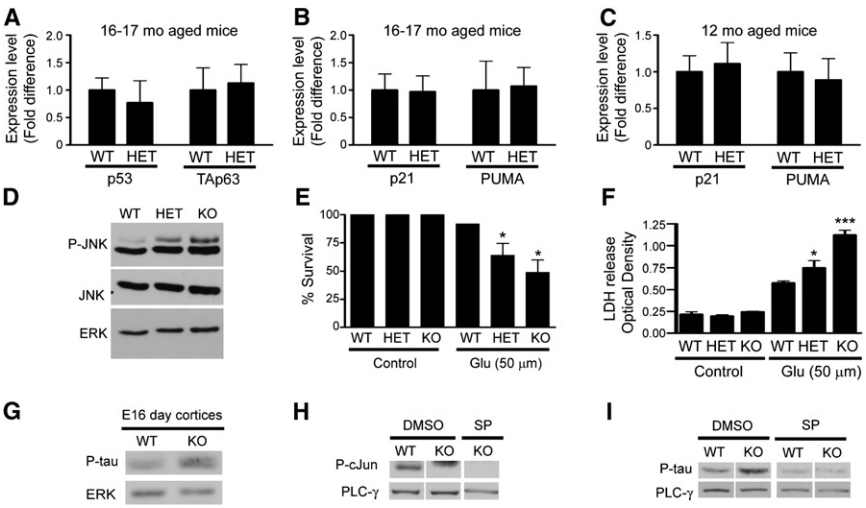

Figure 6. $p73^{+/-}$ Loss of p73 Causes an Increase in JNK Activation and JNK-Mediated Tau Phosphorylation

(A–C) Quantitative RT-PCR analysis for p53, Tap63 and PUMA, and p21, two targets of the p53 family on cerebral cortices from (A and B) 16- to 17-month-old $p73^{+/+}$ and $p73^{+/-}$ mice (C) 12-month-old $p73^{+/+}$ and $p73^{+/-}$ mice, n = 3 for each genotype at each time point.

(D) Western blot analysis of equal amounts of protein from 8 day sister cultures of $p73^{+/+}$, $p73^{+/-}$, and $p73^{-/-}$ embryonic cortical neurons probed for phosphorylated, activated JNK (P-JNK). The blot was reprobed for total JNK, and ERK as loading controls. Similar results were obtained in three independent experiments.

(E and F) $p73^{+/+}$, $p73^{+/-}$, and $p73^{-/-}$ cortical neurons (n = 6 per group from three separate experiments) were exposed to glutamate (Glu) for 24 hr and (E) percent survival was calculated (Hoechst-positive nuclei before and after glutamate), and (F) lactate dehydrogenase (LDH) released into the medium was measured.

(G) Western blot analysis was performed for phosphorylated tau (P-tau) with the AT-8 antibody in embryonic day 16 $p73^{+/+}$ and $p73^{-/-}$ cortices, and the blot was reprobed with ERK as a loading control.

(H and I) Cultured cortical neurons were treated with JNK inhibitor (SP 6000125, 20 μM for 90 min). JNK activity was assessed by western blot analysis for phosphorylated c-*jun* (P-cJun) (H). The effects of JNK inhibition on tau phosphorylation were determined by probing similar western blots with the AT-8 antibody (I). In both cases, blots were reprobed for PLC-γ.

In all panels, WT = $p73^{+/+}$, HET = $p73^{+/-}$, KO = $p73^{-/-}$. Values indicate mean ± SEM. *p < 0.05, ***p < 0.001.

versus 927,555 ± 25,798, respectively; mean ± SEM, n = 4; p < 0.05) (Figure 5I). Silver staining also revealed the presence of degenerating cells, many with dystrophic neurites identifying them as neurons, in the 2-month-old $p73^{+/-}$; TgCRND8$^{+/ø}$ brains (Figure 5J). By 12 months of age, this degeneration was even more dramatic (Figure 5K), with many condensed, dystrophic neurons present throughout the brain and numerous silver stain-positive neurites (Figure 5K). In contrast, only the very occasional silver stain-positive cell was observed in the 12-month-old TgCRND8$^{+/ø}$ brain, although we did observe silver-stained plaques (Figure 5K; data not shown). Thus, p73 haploinsufficiency causes neuronal loss and degeneration coincident with accumulation of P-PHF-tau filaments in an APP-based mouse model of AD.

p73 Modulates JNK Activity to Regulate Neuronal Survival and Tau Phosphorylation

Since ΔNp73 antagonizes proapoptotic p53 family members, one potential explanation for these findings is upregulation of the levels and/or activity of p53 or p63 (Jacobs et al., 2005). However, quantitative RT-PCR (QRT-PCR) of aged $p73^{+/-}$ versus $p73^{+/+}$ cortices demonstrated that levels of p53 and p63 mRNAs, and their downstream targets p21 and PUMA were unaltered by p73 haploinsufficiency (Figures 6A–6C). A second potential explanation involves JNK, since we previously showed that ΔNp73 can bind to and inhibit JNK (Lee et al., 2004), and JNK has been implicated in both neurodegeneration and aberrant tau phosphorylation (reviewed in Johnson and Nakamura, 2007). We therefore measured JNK activity in cultured $p73^{+/+}$, $p73^{+/-}$, and $p73^{-/-}$ cortical neurons. Western blot analysis revealed that levels of the phosphorylated, activated form of JNK increased as the number of wild-type *p73* alleles decreased (Figure 6D). Coincident with this increase in JNK activity, we observed that $p73^{+/-}$ and $p73^{-/-}$ cortical neurons were more vulnerable to death in response to mildly excitotoxic concentrations of the neurotransmitter glutamate (Figures 6E and S5). Measurement of lactate dehydrogenase (LDH) release into the medium, a biochemical indicator of necrosis, demonstrated that, unexpectedly, LDH release increased as *p73* copy number decreased (Figure 6F). Thus, decreased p73 copy number causes increased JNK activity and sensitizes neurons to oxidative damage-induced necrosis.

Since JNK directly phosphorylates tau on residues known to be hyperphosphorylated in P-PHF-tau (Reynolds et al., 1997, 2000; Yoshida et al., 2004), we asked whether JNK dysregulation might also explain the aberrant P-PHF-tau filaments. Western blot analysis revealed increased tau phosphorylation at Ser202/Thr205, targets of JNK-mediated phosphorylation, in neonatal $p73^{-/-}$ versus $p73^{+/+}$ cortices (Figure 6G). To ask whether this tau phosphorylation was JNK dependent, we cultured cortical neurons and treated them for 90 min with the JNK inhibitor SP6000125. SP6000125 decreased phosphorylation of the JNK target, c-*jun*, confirming the efficacy of the inhibitor (Figure 6H). The JNK inhibitor significantly decreased tau phosphorylation in both $p73^{+/+}$ and $p73^{-/-}$ neurons (Figure 6I).

These data indicate that loss of p73 causes increased JNK activity and tau phosphorylation in cultured neurons. To ask whether JNK dysregulation might also explain the phenotypes documented here, we performed double-label immunocytochemistry for phospho-JNK and P-PHF-tau in the 2-month-old $p73^{+/-}$; TgCRND8$^{+/ø}$ cortex. Few phospho-JNK-positive neurons were seen in the TgCRND8 brains at this age, as previously

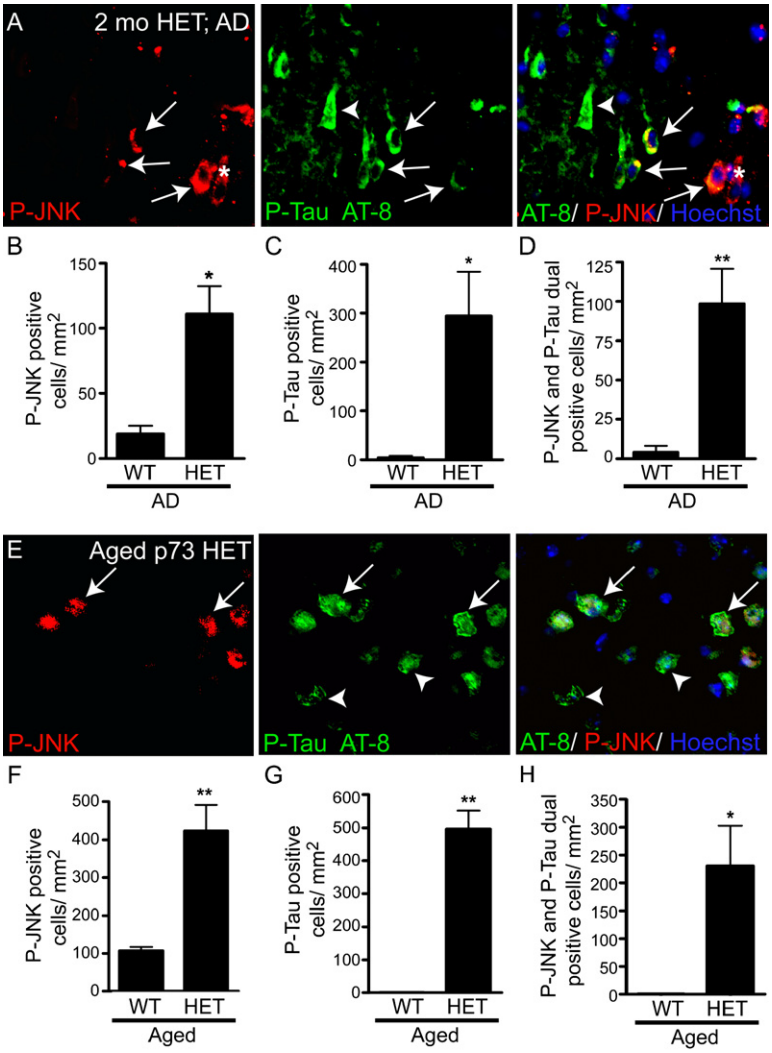

Figure 7. p73 Haploinsufficiency Causes Aberrant JNK Activation in P-PHF-Tau-Positive Neurons in the Aged and AD Brain

(A) Representative photomicrographs of coronal sections of the 2-month-old $p73^{+/-}$;TgCRND8$^{+/\varnothing}$ lateral cortex double labeled for P-JNK (red; left panel), and P-PHF-tau with the AT-8 antibody (green, center panel; right panel is the merge, including the Hoechst counterstain in blue). Arrows denote double-labeled cells, the arrowhead a P-PHF-tau-positive cell, and the asterisk a P-JNK-positive cell.

(B–D) Cortical sections immunostained as in (A) were quantified to determine the number of cells that were positive for (B) P-JNK alone, (C) P-tau alone, and (D) P-JNK and P-tau double-labeled cells.

(E) Representative photomicrographs of coronal sections of the 16- to 17-month-old $p73^{+/-}$ lateral cortex double labeled for P-JNK (red; left panel), and P-PHF-tau with the AT-8 antibody (green, center panel; right panel is the merge, including the Hoechst counterstain in blue). Arrows denote double-labeled cells, and arrowhead P-PHF-tau-positive cells.

(F–H) Cortical sections immunostained as in (A) were quantified to determine the number of cells that were positive for (B) P-JNK alone, (C) P-tau alone, and (D) P-JNK and P-tau double-labeled cells. *$p < 0.05$, **$p < 0.001$. $n = 3$ animals from each genotype.

reported (Bellucci et al., 2007). However, the $p73^{+/-}$;TgCRND8$^{+/\varnothing}$ brains contained many phospho-JNK-positive cells (Figure 7A); quantification revealed a 20-fold increase in their density within the lateral cortex (Figure 7B). Most of these phospho-JNK-positive cells were also positive for P-PHF-tau Ser202/Thr205 phosphorylation (Figures 7A–7D). Similar results were obtained in the aged $p73^{+/-}$ brains; many more phospho-JNK-positive cells were present in aged $p73^{+/-}$ versus $p73^{+/+}$ cortices (Figures 7E and 7F), and many of these colocalized with P-PHF-tau Ser202/Thr205 (Figures 7E, 7G, and 7H). Thus, p73 haploinsufficiency causes increased neuronal JNK activity that likely participates in the genesis of P-PHF-tau pathology.

DISCUSSION

The findings presented here support three major conclusions. First, our data demonstrate that haploinsufficiency for *p73* leads to behavioral and anatomical changes indicative of age-related neurodegeneration. Some of these changes, such as increased microglial activation and enhanced lipofuscin, are likely secondary to neuronal degeneration. However, the neuronal cell loss, increased neuronal senescence, increased reentry of neurons into the cell cycle, and accumulation of P-PHF-tau filaments are all likely to be direct effects of the loss of p73. Second, we demonstrate that *p73* haploinsufficiency causes the amyloid-based TgCRND8 AD mouse model to coincidentally develop the three primary pathologies associated with AD—plaques, P-PHF-tau deposits, and neuronal degeneration—at the same early time point. This accumulation of P-PHF-tau deposits is seen as early as 1.5 months, which is much sooner than in either the $p73^{+/-}$ mice or in the TgCRND8 AD mice, indicating that these two phenotypes synergize. These animals therefore represent a new mouse model for AD. Third, our mechanistic studies indicate that haploinsufficiency for p73 likely causes both neuronal degeneration/loss and P-PHF-tau filament accumulation by directly regulating JNK. These findings, together with recent reports that decreased p73 expression occurs in some cases of AD (Li et al., 2004) and that some individuals show loss of one copy of the genomic locus encompassing the p73 gene (Wong et al., 2007), suggest that haploinsufficiency for p73 may represent a previously unrecognized susceptibility factor for AD.

One surprising result of our study was the occurrence in aged $p73^{+/-}$ mice of multiple hallmarks of neurodegeneration, including phosphorylated tau tangle-like structures, lipofuscin deposits, activation of microglia, cellular senescence, and aberrant entry of neurons into the cell cycle. Aberrant tau regulation is prominent in dementias such as AD (reviewed in Johnson and Stoothoff, 2004), and buildup of lipofuscin causes Batten's disease, an inherited disease with premature dementia (reviewed in Haltia et al., 2006). Microglia likely contribute to

neurodegeneration, since immunosuppression decreases tangles and neuronal loss and increases lifespan in mice expressing mutant tau (Yoshiyama et al., 2007). Reentry of neurons into the cell cycle has been noted in early-stage AD (reviewed in Herrup and Yang, 2007), and postmitotic neurons forced to reenter the cell cycle die by p53-dependent apoptosis (reviewed in Jacobs et al., 2006). Cellular senescence is also associated with aging in mammals. While neurons are postmitotic, and senescence involves cell cycle arrest, these two states are not necessarily equivalent, and it is possible that postmitotic neurons directly enter a senescent state as a consequence of accumulated DNA damage. Alternatively, damaged neurons may aberrantly reenter the cell cycle, as observed here, and perhaps it is this population that then enters a senescent state. In either case, these senescent neurons are abnormal and may well contribute to the pathology described here. Thus, aged $p73^{+/-}$ brains show all of the hallmarks of a neurodegenerative phenotype.

How does *p73* haploinsufficiency cause neurodegeneration? A characteristic of the aging brain is increased vulnerability to toxic insults such as oxidative stress and the resultant DNA damage. In this regard, we show here that loss of one or two alleles of *p73* markedly enhances the vulnerability of CNS neurons to excitotoxicity-induced necrotic cell death, and we have previously shown that overexpression of truncated ΔNp73 protects neurons from DNA damage-induced apoptosis (Pozniak et al., 2002; Walsh et al., 2004). We propose that the neurodegeneration phenotypes reported here are the result of reduced ΔNp73 levels, which is the only detectable p73 isoform in the postnatal mouse CNS (Pozniak et al., 2000). ΔNp73 binds to and suppresses the activity of two important regulators of neural death, p53 (Pozniak et al., 2000) and JNK (Lee et al., 2004), and data presented here indicate that it is the latter pathway that is perturbed in the aged $p73^{+/-}$ brain. This aberrant JNK activation would sensitize cells to oxidative damage, ultimately causing cell senescence and loss (Yang et al., 1997). JNK is also a tau kinase (Reynolds et al., 1997, 2000; Yoshida et al., 2004), and, as seen here, aberrant upregulation of tau phosphorylation likely causes genesis of P-PHF-tau filaments, which may themselves cause neuronal degeneration.

A second surprising finding of our study is that the combination of *p73* haploinsufficiency and overexpression of mutant APP causes neurodegeneration and P-PHF-tau accumulation much earlier than is seen in either genotype alone, suggesting that these two insults synergize. The resultant mouse therefore mimics human AD, demonstrating coincident neuronal loss, and plaque and P-PHF-tau filament formation, without the necessity of tau overexpression. Interestingly, genetic deletion of Pin1, a prolyl isomerase that stabilizes p73, also causes neurodegeneration and accumulation of P-PHF-tau (Liou et al., 2003). Why do these two genetic alterations together cause an early AD-like phenotype? We propose that p73 haploinsufficiency and β-amyloid accumulation converge to upregulate JNK activity in neurons. This convergent JNK dysregulation would presumably cause early dysregulation of tau phosphorylation and increased sensitivity to the toxic effects of β-amyloid and other oxidative stresses (reviewed in Johnson and Nakamura, 2007). The net predicted result would be neurodegeneration at time points much earlier than seen with either genetic insult individually, as reported here.

These data, and the recent association between decreased ΔNp73 and AD (Li et al., 2004), suggest that those individuals with copy number variations at the p73 genomic locus (Wong et al., 2007) may be at enhanced risk for development of AD or other neurodegenerative disorders. We predict that this population would also be more vulnerable to age-related neurodegeneration or other degenerative disorders such as Parkinson's disease. It will be interesting to test this prediction and to determine whether haploinsufficiency for *p73* will exacerbate the degeneration phenotype of mouse models of other human diseases.

EXPERIMENTAL PROCEDURES

Animals

This study was approved by The Hospital for Sick Children's Animal Care Committee, and use was in accordance with CCAC guidelines. $p73^{+/-}$ transgenic mice (Yang et al., 2000) were maintained on a C129SvJae background, as described (Pozniak et al., 2000, 2002). TgCRND8 hemizygous mice containing the Swedish (K670N/M671L) and Indiana (V717F) APP mutations were maintained on a C129 background, as described (Chishti et al., 2001). TgCRND8 hemizygous mice were crossed with $p73^{+/-}$ transgenic mice to generate F1 $p73^{+/-}$; TgCRND8$^{+/\varnothing}$ and $p73^{+/+}$; TgCRND8$^{+/\varnothing}$ mice for analysis.

Primary Neuron Cultures

Embryonic cortical cultures were prepared as described (Lee et al., 2004). For cell death experiments, 50 μM glutamate was added at 7 DIV, and nuclei were labeled with Hoechst 33258 (1:2000). LDH release was assayed as described (Wetzel et al., 2003). JNK was inhibited with SP6000125 (AG Scientific, San Diego, CA).

Behavioral Studies

All behavioral testing took place under dim lighting and constant background noise. Mice were handled 4 min a day for 7 days and habituated to the test environment prior to testing. Groups of 15 to 20 mice were tested sequentially and were handled, habituated, trained, and tested at the same time of day for each experiment. Behavioral tests were run in order from least to most stressful, i.e., limb clasping, paw grip endurance, open-field, water maze. Details of behavioral tests are described in Supplemental Data.

Neuroanatomy

For histology, mice were sacrificed by sodium pentobarbital overdose and transcardially perfused with PBS followed by 4% paraformaldehyde. Tissues were cryoprotected and sectioned at 16 μm or 20 μm for brains and penises, respectively. Nissl staining and immunocytochemistry were performed as described (Pozniak et al., 2002). Endogenous lipofuscin autofluorescence was quenched using Autofluorescence Eliminator (Chemicon, Temecula, CA). Antibodies are listed in Supplemental Data. Immunoreactivity was visualized using CY-3 or FITC conjugated secondary antibodies (1:250, Jackson ImmunoResearch Labs, West Grove, PA) and nuclei labeled with Hoechst 33258 (1:2000, Sigma). SA-β-gal staining was performed as described (Dimri et al., 1994). To detect argyrophilic, degenerating neurons, silver staining was performed using the FD NeuroSilver kit II (FD Neurotech, Ellicott City, MD). Neuroanatomical parameters were measured in the motor cortex at the same rostrocaudal level and were quantified in a strip of cortical tissue 325 μm wide spanning from corpus callosum to pial surface as shown in Figure 2B. Cell and fluorescence density were calculated using these area, cell count, and fluorescence measurements (Pozniak et al., 2002). All digital image acquisition was performed using Northern Eclipse software (Empix Inc.) linked to a Sony XC-75CE CCD video camera (Tokyo, Japan), and processed by ImageJ analysis software (National Institute of Health).

Stereology

Total neuron number and volumetric density of primary motor cortex neurons were obtained by applying unbiased stereology using the optical fractionator (Gundersen et al., 1988; West et al., 1996; Luk and Sadikot, 2003; Luk et al., 2001) with Stereo Investigator software (Micobrightfield, VT, USA). The rostral and caudal limits of the primary motor cortex were determined (equivalent to Bregma 2.46 to −1.94 mm; Paxinos and Franklin, 2001), and every 55th serial section of 16 μm within this volume was examined. Typically, six coronal sections at 880 μm intervals were analyzed throughout the reference volume. Mean section thickness after Cresyl Violet processing, mounting, and coverslipping was 10 μm (tissue shrinkage effect), as measured with a z axis microcator. Sampling of the primary motor cortex was performed by randomly translating a grid with 300 × 300 μm squares onto the section of interest and applying an optical dissector consisting of an 80 × 80 × 6 μm brick. Sections were analyzed by using a ×100 lens (oil, numerical aperture of 1.3, with matching condenser). The most prominent nucleolus was taken as the unique identifier in all sections stained for Nissl substance.

Magnetic Resonance Imaging

For MRI, mice were perfusion fixed, decapitated, and skinned skulls were incubated in ProHance contrasting reagent (Henkelman et al., 2006; Spring et al., 2007). Prior to imaging, samples were removed from the contrast agent solution, blotted, and placed into 13 mm diameter plastic tubes filled with a proton-free susceptibility-matching fluid (Fluorinert FC-77, 3M Corp., St. Paul, MN). Digital anatomical images of brains within skulls were acquired with a multichannel 7.0 Tesla MRI scanner (Varian Inc., Palo Alto, CA) with a 6 cm inner bore diameter insert gradient set. Three brains were imaged in parallel using custom-built, 14 mm diameter solenoid coils with a length of 18.3 cm and over wound ends. The parameters used in the scans were optimized for gray/white matter contrast: a T2-weighted, 3D fast spin-echo sequence, with TR/TE = 325/32 ms, four averages, field-of-view 12 × 12 × 25 mm, and matrix size = 432 × 432 × 780 giving an image with 32 μm isotropic voxels[35]. Total imaging time was 11.3 hr. Geometric distortion due to position of the three coils inside the magnet was corrected using an MR phantom. An unbiased model-independent atlas of the MR scans was created as previously described (Spring et al., 2007) and detailed in Supplemental Data.

Flow Cytometry of DNA Content

One cortical hemisphere per animal (n = 6 per group) was minced, dissociated with papain (2.5 U/ml, Worthington Biochemicals, Lakewood, NJ), dispase (1 U/ml, Sigma), and DNase I (250 U/ml, Sigma) for 30 min at 37°C, triturated in DMEM containing 10% FBS, and fixed with 70% ethanol. Cells were blocked using the Mouse-on-Mouse (MOM) kit (Vector labs, Burlington, ON, Canada), and immunolabeling was performed with monoclonal mouse anti-NeuN (1:100; Chemicon), biotinylated anti-mouse IgG secondary, and Streptavidin conjugated FITC (1:400; Becton Dickson, Mississauga, ON, Canada). Samples were incubated with propidium iodide (50 μg/ml, Sigma) and RNase A (2 mg/ml, Fermentas, Burlington, ON, Canada), and analyzed using a FACScan (Becton Dickinson, Franklin Lakes, NJ) and FlowJo software (Tree Star, Inc., Ashland, Oregon), gating for single cells.

Electron Microscopy

Mice were sacrificed by sodium pentobarbital overdose and transcardially perfused with 4% PFA and 0.1% glutaraldehyde in 0.1 M phosphate buffer, pH 7.4. The tissue was dehydrated, infiltrated with LR White, 80 nm sections were placed on Formvar-coated nickel grids, incubated with P-PHF-tau (AT-8; 1:10), which was detected using goat anti-mouse gold conjugate secondary antibodies (10 nm gold; 1:20, Jackson ImmunoResearch Labs), fixed 10 min with 2% glutaraldehyde, stained with uranyl acetate, and lead citrate. The sections were examined using an FEI Tecnai 20 transmission electron microscope (FEI Company, Hillsboro, OR), and images were captured using a Gatan Dualview digital camera (Gatan Inc, Pleasanton, CA).

Quantitative RT-PCR

Total RNA was extracted from each cortex using Trizol reagent (Invitrogen) and the RNeasy kit (QIAGEN). cDNA was prepared with SuperScript III First-Strand Synthesis SuperMix for qRT-PCR (Invitrogen). Real-time PCR was performed according to the manufacturers' specifications using Chromo4 Real-Time PCR Detection System (Bio-Rad) and a Platinum Quantitative PCR SuperMix-UDG (Invitrogen). Samples were analyzed in triplicate and were normalized to β-actin for each reaction. The primers are detailed in Supplemental Data. All PCR products were single bands with predicted molecular weights.

Phosphatase Treatment

To determine specificity of P-PHT-tau antibodies, fixed brain sections were dephosphorylated and then labeled with P-PHF-tau antibody AT-180 as previously described (Papasozomenos and Binder, 1987; Yang et al., 2003) and described in Supplemental Data.

Biochemistry and Western Blot Analysis

Western blot analyses of cultured cortical neurons were performed as previously described (Lee et al., 2004). Antibodies are in Supplemental Data. To detect P-PHF-tau in aged mouse brain, a P-PHF-tau enriched fraction was generated from 18-month-old $p73^{+/-}$ and $p73^{+/+}$ mice as previously described (Ikeda et al., 2005).

Statistics

Data are expressed as means ± SEM. Significant differences between means were determined using t tests or one-way analysis of variance.

SUPPLEMENTAL DATA

The Supplemental Data include figures, movies, and Supplemental Experimental Procedures and can be found with this article online at http://www.neuron.org/cgi/content/full/59/5/708/DC1/.

ACKNOWLEDGMENTS

This work was funded by grants from the CIHR and NeuroScience Canada. We thank R. Temkin and the Advanced Bioimaging Centre of the HSC Research Institute for immuno-EM, Frank McKeon (Harvard University) for the generous gift of the p73 knockout mice, and David Westaway (University of Alberta) for the generous gift of the TgCRND8 mice. M.K.W. has a fellowship from CIHR/Heart & Stroke and J.A.B. and J.P.L. from CIHR. F.D.M. is an HHMI International Research Scholar, and R.M.H., F.D.M., and D.R.K. hold CRC chairs.

Accepted: July 8, 2008
Published: September 10, 2008

REFERENCES

Ballatore, C., Lee, V.M., and Trojanowski, J.Q. (2007). Tau-mediated neurodegeneration in Alzheimer's disease and related disorders. Nat. Rev. Neurosci. *8*, 663–672.

Bellucci, A., Rosi, M.C., Grossi, C., Fiorentini, A., Luccarini, I., and Casamenti, F. (2007). Abnormal processing of tau in the brain of aged TgCRND8 mice. Neurobiol. Dis. *27*, 328–338.

Chishti, M.A., Yang, D.S., Janus, C., Phinney, A.L., Horne, P., Pearson, J., Strome, R., Zuker, N., Loukides, J., French, J., et al. (2001). Early-onset amyloid deposition and cognitive deficits in transgenic mice expressing a double mutant form of amyloid precursor protein 695. J. Biol. Chem. *276*, 21562–21570.

Dimri, G.P., Lee, X., Basile, G., Acosta, M., Scott, G., Roskelley, C., Medrano, E.E., Linskens, M., Rubelj, I., Pereira-Smith, O., et al. (1994). A biomarker that identifies senescent human cells in culture and in aging skin in vivo. Proc. Natl. Acad. Sci. USA *92*, 9363–9376.

Dusart, I., Guenet, J.L., and Sotelo, C. (2006). Purkinje cell death: differences between developmental cell death and neurodegenerative death in mutant mice. Cerebellum *5*, 163–173.

Goedert, M., Jakes, R., and Vanmechelen, E. (1995). Monoclonal antibody AT8 recognises tau protein phosphorylated at both serine 202 and threonine 205. Neurosci. Lett. *189*, 167–169.

Goldstein, D.S. (2003). Dysautonomia in Parkinson's disease: neurocardiological abnormalities. Lancet Neurol. *2*, 669–676.

Gundersen, H.J., and Jensen, E.B. (1987). The efficiency of systematic sampling in stereology and its prediction. J. Microsc. *147*, 229–263.

Gundersen, H.J., Bagger, P., Bendtsen, T.F., Evans, S.M., Korbo, L., Marcussen, N., Moller, A., Nielsen, K., Nyengaard, J.R., Pakkenberg, B., et al. (1988). The new stereological tools: dissector, fractionator, nucleator and point sampled intercepts and their use in pathological research and diagnosis. APMIS *96*, 857–881.

Haltia, M. (2006). The neuronal ceroid-lipofuscinoses: from past to present. Biochim. Biophys. Acta. *1762*, 850–856.

Hawkes, C. (2006). Olfaction in neurodegenerative disorders. Adv. Otolaryngology *63*, 133–151.

Henkelman, R.M., Dazai, J., Lifshitz, N., Nieman, B.J., Tsatskis, S., Lerch, J., Bishop, S., Kale, S., Sled, J.G., and Chen, X.J. (2006). High throughput microimaging of the mouse brain. In: Proceedings of the 14th Annual Meeting of ISMRM, Seattle, WA, USA.

Herrup, K., and Yang, Y. (2007). Cell cycle regulation in the postmitotic neuron: oxymoron or new biology? Nat. Rev. Neurosci. *8*, 368–378.

Ikeda, M., Shoji, M., Kawarai, T., Kawarabayashi, T., Matsubara, E., Murakami, T., Sasaki, A., Tomidokoro, Y., Ikarashi, Y., Kuribara, H., et al. (2005). Accumulation of filamentous tau in the cerebral cortex of human tau R406W transgenic mice. Am. J. Pathol. *166*, 521–531.

Imhof, A., Kovari, E., von Gunten, A., Gold, G., Rivara, C.B., Herrmann, F.R., Hof, P.R., Bouras, C., and Giannakopoulos, P. (2007). Morphological substrates of cognitive decline in nonagenarians and centenarians: a new paradigm? J. Neurol. Sci. *257*, 72–79.

Jacobs, W.B., Govoni, G., Ho, D., Atwal, J.K., Barnabé-Heider, F., Keyes, W.M., Mills, A.A., Miller, F.D., and Kaplan, D.R. (2005). p63 is an essential proapoptotic protein during neural development. Neuron *48*, 743–756.

Jacobs, W.B., Kaplan, D.R., and Miller, F.D. (2006). The p53 family in nervous system development and disease. J. Neurochem. *97*, 1571–1584.

Johnson, G., and Stoothoff, W.H. (2004). Tau phosphorylation in neuronal cell function and dysfunction. J. Cell Sci. *117*, 5712–5729.

Johnson, G.L., and Nakamura, K. (2007). The c-jun kinase/stress-activated pathway: regulation, function, and role in human disease. Biochim. Biophys. Acta *1773*, 1341–1348.

Keyes, W.M., Wu, Y., Vogel, H., Guo, X., Lowe, S.W., and Mills, A.A. (2005). p63 deficiency activates a program of cellular senescence and leads to accelerated aging. Genes Dev. *19*, 1986–1999.

Kobayashi, D.T., and Chen, K.S. (2005). Behavioral phenotypes of amyloid-based genetically modified mouse models of Alzheimer's disease. Genes Brain Behav. *4*, 173–196.

Lavigueur, A., Maltby, V., Mock, D., Rossant, J., Pawson, T., and Bernstein, A. (1989). High incidence of lung, bone, and lymphoid tumours in transgeniuc mice over-expressing mutant alleles of the p53 oncogene. Mol. Cell. Biol. *9*, 3982–3991.

Lee, A.F., Ho, D.K., Walsh, G.S., Kaplan, D.R., and Miller, F.D. (2004). Evidence for a ΔNp73:p53 survival checkpoint upstream of the mitochondrion. J. Neurosci. *24*, 9174–9184.

Lewis, J., McGowan, E., Rockwood, J., Melrose, H., Nacharaju, P., Van Slegtenhorst, M., Gwinn-Hardy, K., Paul Murphy, M., Baker, M., Yu, X., et al. (2000). Neurofibrillary tangles, amyotrophy and progressive motor disturbance in mice expressing mutant (301L) tau protein. Nat. Genet. *25*, 402–405.

Li, Q., Athan, E.S., Wei, M., Yuan, E., Rice, S.L., Vonsattel, J.P., Mayeux, R.P., and Tycko, B. (2004). TP73 allelic expression in human brain and allele frequencies in Alzheimer's disease. BMC Med. Genet. *5*, 14.

Lin, M.T., and Beal, M.F. (2006). Mitochondrial dysfunction and oxidative stress in neurodegenerative diseases. Nature *443*, 787–795.

Liou, Y.C., Sun, A., Ryo, A., Zhou, X.Z., Yu, Z.X., Huang, H.K., Uchida, T., Bronson, R., Bing, G., Li, X., et al. (2003). Role of the prolyl isomerase Pin1 in protecting against age-dependent neurodegeneration. Nature *424*, 556–561.

Luk, K.C., and Sadikot, A.F. (2003). GABA promotes survival but not proliferation of parvalbumin-immunoreactive interneurons in rodent neostriatum: an in vivo study with stereology. Neuroscience *104*, 93–103.

Luk, K.C., Kennedy, T., and Sadikot, A.F. (2001). Glutamate promotes proliferation of striatal neuronal progenitors by an NMDA receptor-mediated mechanism. J. Neurosci. *23*, 2239–2250.

Maier, B., Gluba, W., Bernier, B., Turner, T., Mohammad, K., Guise, T., Sutherland, A., Thorner, M., and Scrable, H. (2004). Modulation of mammalian life span by the short isoform of p53. Genes Dev. *18*, 306–319.

Papasozomenos, S.C., and Binder, L.I. (1987). Phosphorylation determines two distinct species of Tau in the central nervous system. Cell Motil. Cytoskeleton *8*, 210–226.

Papazoglu, C., and Mills, A.A. (2007). p53: at the crossroad between cancer and ageing. J. Pathol. *211*, 124–133.

Parkes, T.L., Elia, A.J., Dickinson, D., Hilliker, A.J., Phillips, J.P., and Boulianne, G.L. (1998). Extension of Drosophila lifespan by overexpression of human SOD1 in motor neurons. Nat. Genet. *19*, 171–174.

Paxinos, G., and Franklin, K.B.J. (2001). The Mouse Brain in Stereotaxtic Coordinates, Second Edition (San Francisco: Academic Press).

Pozniak, C.D., Radinovic, S., Yang, A., McKeon, F., Kaplan, D.R., and Miller, F.D. (2000). An anti-apoptotic role for the p53 family member, p73, during developmental neuron death. Science *289*, 304–306.

Pozniak, C.D., Barnabé-Heider, F., Rymar, V.V., Lee, A.F., Sadikot, A.F., and Miller, F.D. (2002). p73 is required for survival and maintenance of cortical neurons. J. Neurosci. *22*, 9800–9809.

Reynolds, C.H., Utton, M.A., Gibb, G.M., Yates, A., and Anderton, B.H. (1997). Stress-activated protein kinase/c-jun N-terminal kinase phosphorylates tau protein. J. Neurochem. *68*, 1736–1744.

Reynolds, C.H., Betts, J.C., Blackstock, W.P., Nebreda, A.R., and Anderton, B.H. (2000). Phosphorylation sites on tau identified by nanoelectrospray mass spectrometry: differences in vitro between the mitogen-activated protein kinases ERK2, c-jun N-terminal kinase and P38, and glycogen synthase kinase-3beta. J. Neurochem. *74*, 1587–1595.

Seehafer, S.S., and Pearce, D.A. (2006). You say lipofuscin, we say ceroid: defining autofluorescent storage material. Neurobiol. Aging *27*, 576–588.

Serrano, M., Lin, A.W., McCurrach, M.E., Beach, D., and Lowe, S.W. (1997). Oncogenic ras provokes premature cell senescence associated with accumulation of p53 and $p16^{INK4a}$. Cell *88*, 593–602.

Spring, S., Lerch, J., and Henkelman, R.M. (2007). Sexual dimorphism revealed in the structure of the mouse brain using three-dimensional magentic resonance imaging. Neuroimage *35*, 1424–1433.

Talos, F., Nemajerova, A., Flores, E.R., Petrenko, O., and Moll, U.M. (2007). p73 suppresses polyploidy and aneuploidy in the absence of functional p53. Mol. Cell *27*, 647–659.

Tyner, S.D., Venkatachalam, S., Choi, J., Jones, S., Ghebranious, N., Igelmann, H., Lu, X., Soron, G., Cooper, B., Brayton, C., et al. (2002). p53 mutant mice that display early ageing-associated phenotypes. Nature *415*, 45–53.

Walsh, G.S., Orike, N., Kaplan, D.R., and Miller, F.D. (2004). The invulnerability of adult neurons: a critical role for p73. J. Neurosci. *24*, 9638–9647.

West, M.J., Ostergaard, K., Andreassen, O.A., and Finsen, B. (1996). Estimation of the number of somatostatin neurons in the striatum: an in situ hybridization study using the optical fractionator method. J. Comp. Neurol. *370*, 11–22.

Wetzel, M., Rosenberg, G.A., and Cunningham, L.A. (2003). Tissue inhibitor of metalloproetinases-3 and matrix metalloproteinase-3 regulate neuronal sensitivity to doxorubicin-induced apoptosis. Eur. J. Neurosci. *18*, 1050–1060.

Wong, K.K., deLeeuw, R.J., Dosanjh, N.S., Kimm, L.R., Cheng, Z., Horsman, D.E., MacAulay, C., Ng, R.T., Brown, C.J., Eichler, E.E., and Lam, W.L. (2007). A comprehensive analysis of common copy-number variations in the human genome. Am. J. Hum. Genet. *80*, 91–104.

Yang, D.D., Kuan, C.Y., Whitmarsh, A.J., Rincón, M., Zheng, T.S., Davis, R.J., Rakic, P., and Flavell, R.A. (1997). Absence of excitotoxicity-induced apoptosis in the hippocampus of mice lacking the Jnk3 gene. Nature *389*, 865–870.

Yang, A., Walker, N., Bronson, R., Kaghad, M., Oosterwegel, M., Bonnin, J., Vagner, C., Bonnet, H., Dikkes, P., Sharpe, A., et al. (2000). p73-deficient mice have neurological, pheromonal and inflammatory defects but lack spontaneous tumors. Nature *404*, 99–103.

Yang, W., Sopper, M.M., Leystra-Lantz, C., and Strong, M.J. (2003). Microtubule-associated tau protein positive neuronal and glial inclusions in ALS. Neurology *61*, 1766–1773.

Yoshida, H., Hastie, C.J., Mclauchlan, H., Cohen, P., and Goedert, M. (2004). Phosphorylation of microtubule-associated protein tau by isoforms of c-jun N-terminal kinase (JNK). J. Neurochem. *90*, 352–358.

Yoshiyama, Y., Higuchi, M., Zhang, B., Huang, S.M., Iwata, N., Saido, T.C., Maeda, J., Suhara, T., Trojanowski, J.Q., and Lee, V.M. (2007). Synapse loss and microglial activation precede tangles in a P301S tauopathy mouse model. Neuron *53*, 337–351.

Zhu, X., Raina, A.K., Perry, G., and Smith, M.A. (2006). Apoptosis in Alzheimer disease: a mathematical improbability. Curr. Alzheimer Res. *3*, 393–396.